ELSEVIER

Two-way nested model of mesoscale circulation features in the Ligurian Sea

A. Barth [a,*], A. Alvera-Azcárate [a], M. Rixen [b], J.-M. Beckers [a]

[a] *University of Liège, GeoHydrodynamics and Environment Research, MARE, Institut de Physique B5, Sart Tilman, 4000 Liège, Belgium*
[b] *Southampton Oceanography Centre, European Ways, O14 3ZH Southampton, UK*

Abstract

A coarse resolution primitive equation model of 1/4° resolution is implemented covering the whole Mediterranean Sea. Within this grid a 1/20° resolution model of the Liguro-Provençal basin and the northern part of the Tyrrhenian Sea is embedded. A third fine resolution model of 1/60° is nested in the latter one and simulates the dynamics of the Ligurian Sea. Comparisons between one-way and two-way nesting in simulating the Northern Current (NC) are made. The properties of the Eastern and Western Corsican Current and the Northern Current are investigated with this nesting system. Special attention is given to the variability of the NC. Meanders and interactions with Winter Intermediate Water lenses are shown. Topographic features also lead to a highly variable NC.
© 2005 Elsevier Ltd. All rights reserved.

Keywords: Two-way nested models; Western Corsican Current; Eastern Corsican Current; Northern Current; Ligurian Sea

1. Introduction

A system of nested models is applied to the Mediterranean Sea with two successive zooms of the Liguro-Provençal basin and of the Ligurian Sea. Two strong and variable currents, the Western Corsican Current and the Eastern Corsican Current (hereafter WCC and ECC) enter the domain of the Ligurian Sea (Fig. 1). Both advect Modified Atlantic Water (MAW) at the surface and the ECC also transports the denser Levantine Intermediate Water (LIW). The variability of these currents is investigated by, e.g., Astraldi and Gasparini (1992) and Sammari et al. (1995) and shows a seasonal cycle and a dependence on local

---

* Corresponding author. Present address: Ocean Circulation Group, University of South Florida, College of Marine Science, 140 Seventh Avenue South, 33701 St.Petersburg, FL, USA. Tel.: +1 727 553 3508; fax: +1 727 553 1189.
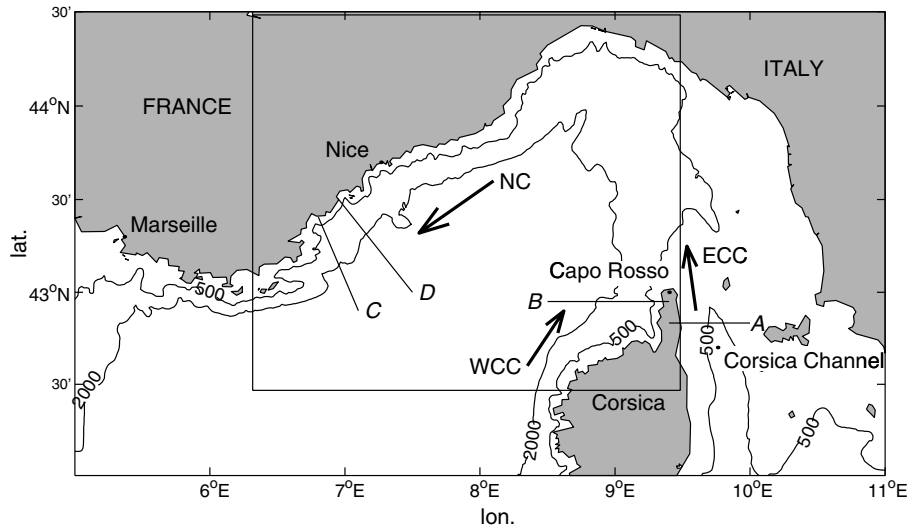 *E-mail address:* abarth@marine.usf.edu (A. Barth).

Fig. 1. The Ligurian Sea with the three major currents: ECC, WCC and NC. The results of the model will be illustrated in sections A, B, C and D. The solid line represents the interface between the fine and intermediate grid resolution models. The 500 and 2000 m isobaths are also shown. While the bathymetry in the Ligurian Sea is rather steep at the French coast, there is a continental shelf in the western part near the Italian coast. The Corisca Channel separates this plateau from the Corsica island.

atmospheric forcings. These currents join and give birth to the Northern Current (hereafter NC) following the French and Spanish coast. NC and WCC describe a cyclonic circulation along the Liguro-Provençal front. Especially during the cold season, a high mesoscale activity associated with meanders in the NC, eddy formation or displacements in the Ligurian-Provençal front can be observed (Sammari, Millot, & Prieur, 1995).

Surface cooling and mixing can transform MAW into Winter Intermediate Water (WIW) that reaches the buoyancy equilibrium between the MAW and the LIW. This process can be compared to the dense water formation in the Gulf of Lions, but WIW formation occurs for less severe weather conditions and only involves the MAW layer (Gasparini, Zodiatis, Astraldi, Galli, & Sparnocchia, 1999).

The spatial resolution of oceanographic models plays an important role in representing and simulating ocean processes. But most of the time this parameter is constrained by computing capacity rather than by physical arguments. So it is desirable to concentrate the resolution efforts in a particular domain of interest or in a crucial region where important processes for a larger domain occur. Modelling an oceanographic system at variable resolution can thus be achieved by nesting a fine grid model in a coarse grid model. Traditionally (e.g., Fox & Maskell, 1995), we distinguish two types of nesting: (i) one-way or passive nesting and (ii) two-way or interactive nesting. In the former case, the fine grid model's boundary conditions are interpolated from the coarse grid model, but the dynamics of the fine grid model do not influence the evolution of the coarse grid model. The two-way nesting approach allows the fine grid model to give a feedback to the coarse grid model after receiving the boundary conditions from the coarse grid model. For multiple or telescopically nested models, the grid refining procedure is repeated several times.

In oceanography, the one-way nesting technique was first applied by Spall and Robinson (1989) and is now a widespread and operational method for studying ocean system in a subdomain (e.g., Robinson & Sellschopp, 2002; Zavatarelli & Pinardi, 2003). For one-way nesting systems, the coarse grid model and the fine grid model can be implemented independently. This approach is therefore well suited for operational forecasts. Inconsistencies between the fine and coarse model evolution, especially after long term integrations, however, make the application of the boundary conditions a delicate task. Two-way nested

models avoid the divergence between fine and coarse grid model and can reduce the problem of inconsistent boundary conditions.

The interactive nesting technique was tested in idealised experiments (e.g., Blayo & Debreu, 1999; Fox & Maskell, 1995; Ginis, Richardson, & Rothstein, 1998; Spall & Holland, 1991) for different resolution ratios between the fine grid and the coarse grid model. It was shown that propagating features such as a barotropic modon, baroclinic vortex, a meandering front or a Kelvin wave along the equator could enter and exit the fine model. Ginis et al. (1998) pointed out that the solution in the high-resolution model is similar to the solution obtained by a high-resolution model covering the whole domain. Fine grid models following a propagating feature were also implemented (Blayo & Debreu, 1999; Rowley & Ginis, 1999).

Realistic ocean systems were also studied, e.g., the Norwegian Coastal Current by Oey and Chen (1992), the Iceland-Faeroes front by Fox and Maskell (1996) and the tropical Pacific Ocean by Ginis et al. (1998).

The Ligurian Sea was chosen for the present study since the thermohaline structure of the NC is determined in this area. The NC is one of the major currents in the Western Mediterranean Sea and surrounds the area of the Gulf of Lions where Western Mediterranean Deep Water formation occurs in winter. Thus, the NC plays an important role for the preconditioning of the surface water in the Gulf of Lions. The NC may also affect the WIW formation in the Ligurian Sea. Since eddies of WIW sink to a depth of about 200–400 m, they may in return also interact with the NC.

Due to the permanent frontal system, the primary production in the Ligurian Sea is exceptionally high for offshore water. Cetacean species are also more abundant in the Ligurian Sea than in other seas of the Western Mediterranean Basin. This has lead to the instauration of Ligurian Sea Cetacean Sanctuary, which aims at protecting this valuable marine environment. Primary producers are particularly sensitive to the hydrodynamical processes that also indirectly have an impact on higher species.

Beside the physical and biological particularities, the Ligurian Sea is an interesting test area since, to our knowledge, no high-resolution study at 1′ has been realised in the Ligurian Sea. This resolution is achieved by two successive grid refinements of a coarse resolution model of the Mediterranean Sea. The present investigation aims at demonstrating that telescopically and interactively nested models applied to a realistic basin are a robust and powerful tool for simulating small-scale ocean processes induced by larger scale currents and fronts.

Because of the strong winds the mesoscale activity in the Ligurian Sea is generally highest during the winter (Albérola, Millot, & Font, 1995). In order to investigate the mesoscale flow features, a wintertime situation was thus chosen for the model run.

The paper is organised as follows: in Section 2, the characteristics of the hydrodynamic model and the nesting procedure are briefly summarised. Practical aspects of the implementation of the nesting system and the application to the Ligurian Sea, Ligurian-Provençal basin and the Mediterranean Sea are given in Section 3. The improvement of a two-way nested model grid compared to a simply coarse resolution grid and one-way nested grid for modelling the NC are shown in Section 4. In Section 5, we discuss the model results and compare them to measurements and results from surveys carried out in the Ligurian Sea.

2. Model description

The GeoHydrodynamics and Environment Research (GHER) model (Beckers, 1991) is used for the present telescopically nesting implementation. The free surface, hydrostatic, primitive equations under the classical Boussinesq and β-plane approximations are solved. The vertical turbulence is parameterised by a k turbulent kinetic energy closure scheme (Nihoul, Deleersnijder, & Djenidi, 1989). The domain is discretised horizontally along parallels and meridional lines. In the vertical, the model uses a double-sigma coordinate (Beckers, 1991). Scalar variables (elevation, temperature, salinity and turbulent kinetic energy) are discretised at the centre of each grid box and at the interface of each box we define the normal velocity

component (a C-grid in Arakawa nomenclature). For computational efficiency, the baroclinic mode is integrated with a much larger time step than the barotropic mode. All models of the nesting system are integrated with the same time step, i.e., 4 s for the barotropic mode and 80 s for the baroclinic mode. The numerical scheme conserves volume, heat and salt. In addition, the advection scheme is a monotone total variation diminishing (TVD) scheme preserving fronts and gradients. Other details of the GHER model can be found in Beckers et al. (2002).

Although the grid was refined twice, the nesting procedure is explained for clarity in the case of a single nesting. For multiple nesting, subsequent description of the grid configuration, of the boundary condition and the feedback holds for every pair of coarse and embedded finer grid models.

The grid refinement ratio r is supposed to be odd and equal in the both horizontal directions. In this way, each grid value of the overlapping region of the coarse grid coincides with a value of the fine grid (Fig. 2). In the vertical, the grid is not refined. To each double-sigma layer of the coarse grid corresponds one layer in the fine grid at the same depth when the bathymetry is consistent at the boundary.
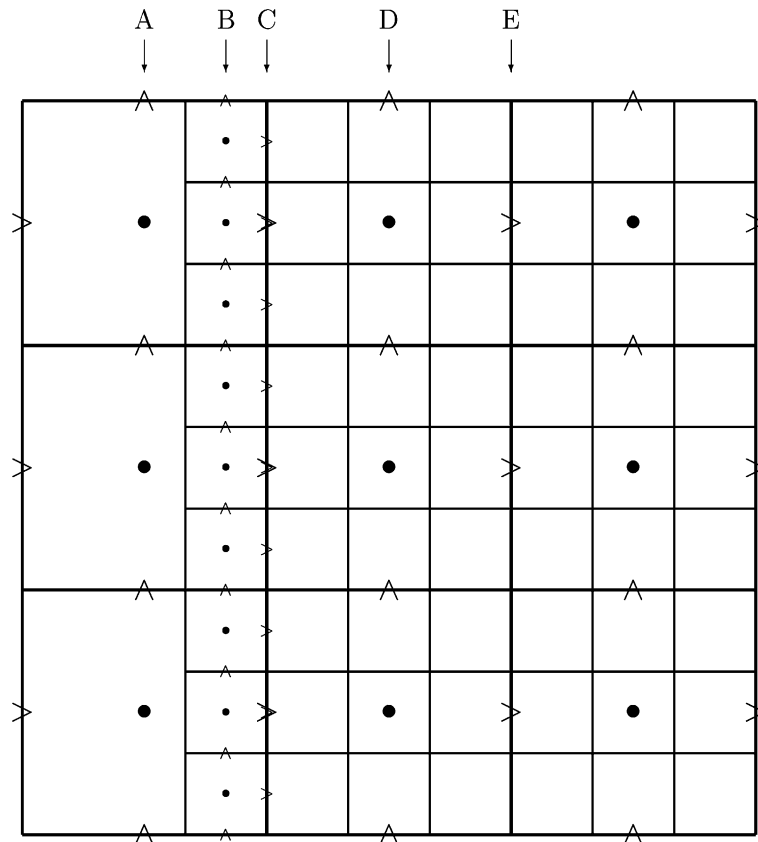

Fig. 2. The relative position of the coarse (heavy lines) and fine grid (fine lines). The dots (•) show the position of scalar variables, > the zonal velocity and ∧ the meridional velocity component. The large symbols are associated to the coarse grid and the small symbols to the fine grid. For clarity, only the position of the variables imposed by boundary conditions are showed for the fine grid. The boundary conditions of the scalars and the tangent (to the nesting boundary) velocities interpolated from columns A and D are imposed in column B. The normal velocity component is imposed in column C. The average values of the scalars and the tangent velocities are injected in the coarse grid model, starting with column D. For the normal velocity, the feedback begins with column E.

Furthermore, the interpolation of the boundary conditions and the feedback procedure are simplified by using a land mask of the fine grid that is equal to the land mask of the overlapping coarse grid for the first $r + 1$ fine grid boxes counted normal to the boundary. The remaining land mask can be chosen to follow as closely as possible the real coastline and the bathymetry.

The nesting procedure and the data flow between the coarse and fine grid models can be summarised as follows. For each variable, we:

(1) interpolate the fine grid boundary conditions for that variable from the coarse grid model and impose the boundary conditions to the fine grid model in the so-called "dynamic interface",
(2) integrate the coarse and fine grid models one time step ahead,
(3) average the values of the fine grid model lying on and inside the "feedback interface" and replace the corresponding values of the coarse grid model. The feedback is thus performed over the entire volume of the nest delimited by the feedback interface.

Fig. 2 shows the position of the dynamic and feedback interface for the different variables, as will be explained in the subsequent sections. For multiple nesting, the feedback starts with the finest embedded model and its average field replaces the values of the next coarsest model. The interested reader may refer to Appendix 1 for details of the nesting procedure.

3. Implementation

Numerous idealised nesting experiments (e.g., Spall & Holland, 1991) show that for a fixed resolution of the fine grid model, acceptable results are obtained for a 3 and 5 times coarser large scale model. With higher nesting ratios, substantial degradation is observed. To achieve a high resolution at regional scales ($1'$) in the Mediterranean Sea, a multiple nesting strategy was thus adopted: a fine resolution ($1'$) regional model of the Ligurian Sea ($6°19'$E to $9°29'$E, $42°28'$N to $44°29'$N) embedded in an intermediate resolution ($3'$) model of the Liguro-Provençal sub-basin ($2°51'$E to $12°9'$, $41°51'$N to $44°39'$N) nested in a coarse resolution ($15'$) general circulation model implemented for the whole Mediterranean Sea (Fig. 3). The main parameters of the three models are given in Table 1.
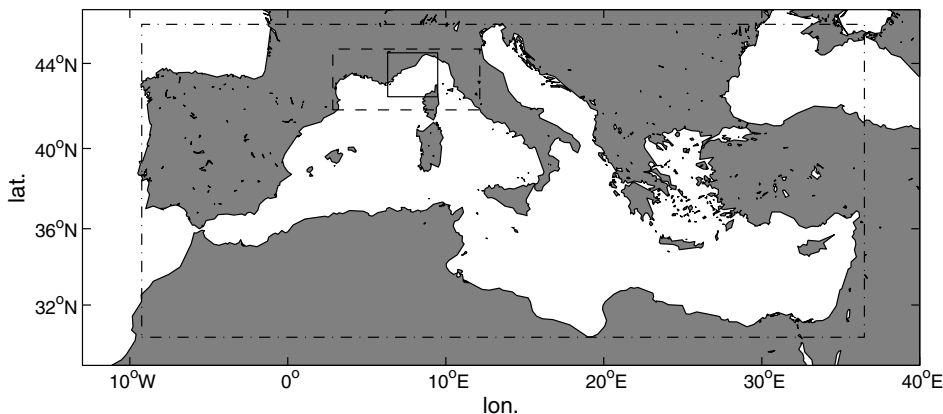

Fig. 3. Domain of the three models. The Mediterranean Sea model is delimited by the dashed line. The dotted line represents the boundary of the Liguro-Provençal model. The Ligurian Sea model lies inside the solid line rectangle.

Table 1
The main parameters of the Mediterranean Sea, the Liguro-Provençal and the Ligurian Sea model

	Mediterranean Sea	Liguro-Provençal basin	Ligurian Sea
Resolution	$15'$	$3'$	$1'$
Δx (m)	21,930	4386	1462
Δy (m)	27,829	5566	1855
Eddy viscosity (m²/s)	200	8	0.9
Eddy diffusivity (m²/s)	60	2.4	0.27

Δx and Δy are the grid spacing in zonal and meridional direction. The β-planes of the three grids are tangent to the Earth at a latitude of 38°.

During winter, the first internal Rossby Radius of deformation is of the order of 4–7 km in the Ligurian Sea (computed form the Mediterranean Oceanic Data Base (MODB) Climatology (Brasseur, Beckers, Brankart, & Schoenauen, 1996; Rixen, Beckers, Brankart, & Brasseur, 2000)) and the associated wavelength is of order 25–44 km. Eddies are thus well resolved in the intermediate resolution and fine resolution models.

The model bathymetry is computed from the Smith and Sandwell (1997) bathymetry. The depth of a coarser mesh box is set equal to the mean depth of the corresponding finer grid mesh. Due to the steep bathymetry near the Western Corsican Coast, the WCC appears to be very sensitive to the difference of the bathymetry of the nesting boundary. Unphysical results may be obtained when a sigma level of the coarse grid is connected to a sigma level of different depth. Near the coast this difference can reach several hundred meters. For simplicity, we impose that the bathymetry in the $r + 1$ first grid points is equal to the bathymetry of the coarse grid model. In principle, this problem could also be solved with a vertical interpolation and sometimes an extrapolation of the boundary condition and the feedback.

The nesting system is forced by National Centers for Environmental Prediction (NCEP, http://www.cdc.noaa.gov/cdc/data.ncep.reanalysis.html) reanalysis atmospheric fluxes. The coarse grid model encompasses some grid points of the Atlantic Ocean. Temperature and salinity at the Atlantic boundary are relaxed to their monthly climatology mean from the MODB and a mean flow is imposed. The freshwater discharge of the Rhône (climatology mean computed from Tusseau & Mouchel, 1994) and the Arno (Rinaldi, pers. commun.) are also included in the intermediate grid size model.

The coarse grid model's initial conditions are also obtained from the MODB Climatology after a 10-year spin-up of the coarse grid model. The initial conditions of the fine grid and intermediate grid are then interpolated. The whole nesting system is spun up during three months using perpetual January 1998 forcings.

The implementation of the nesting system was tested in an idealised, conservative configuration. Without atmospheric and riverine forcings and with the strait of Gibraltar "closed", the nesting system conserves the total volume. As pointed out earlier, temperature and salinity are not conserved by the boundary conditions used is the present implementation. But the losses and gains of these scalars appear to be very small compared to their spatial standard deviation.

4. Comparison between one-way and two-way nesting

The LIW is formed in the Eastern Mediterranean and has travelled a long path before reaching the Ligurian Sea. In the present implementation, the LIW vein crosses the two nested models and is thus particularly sensitive to the nesting strategy used. In order to elucidate the gain of a high-resolution two-way nested model, a one-way nesting experiment was carried out. The parameters, initial conditions and the interpolation of the boundary conditions of the three models are identical to the two-way nesting experiment, but now each model does not depend on the finer resolution model.
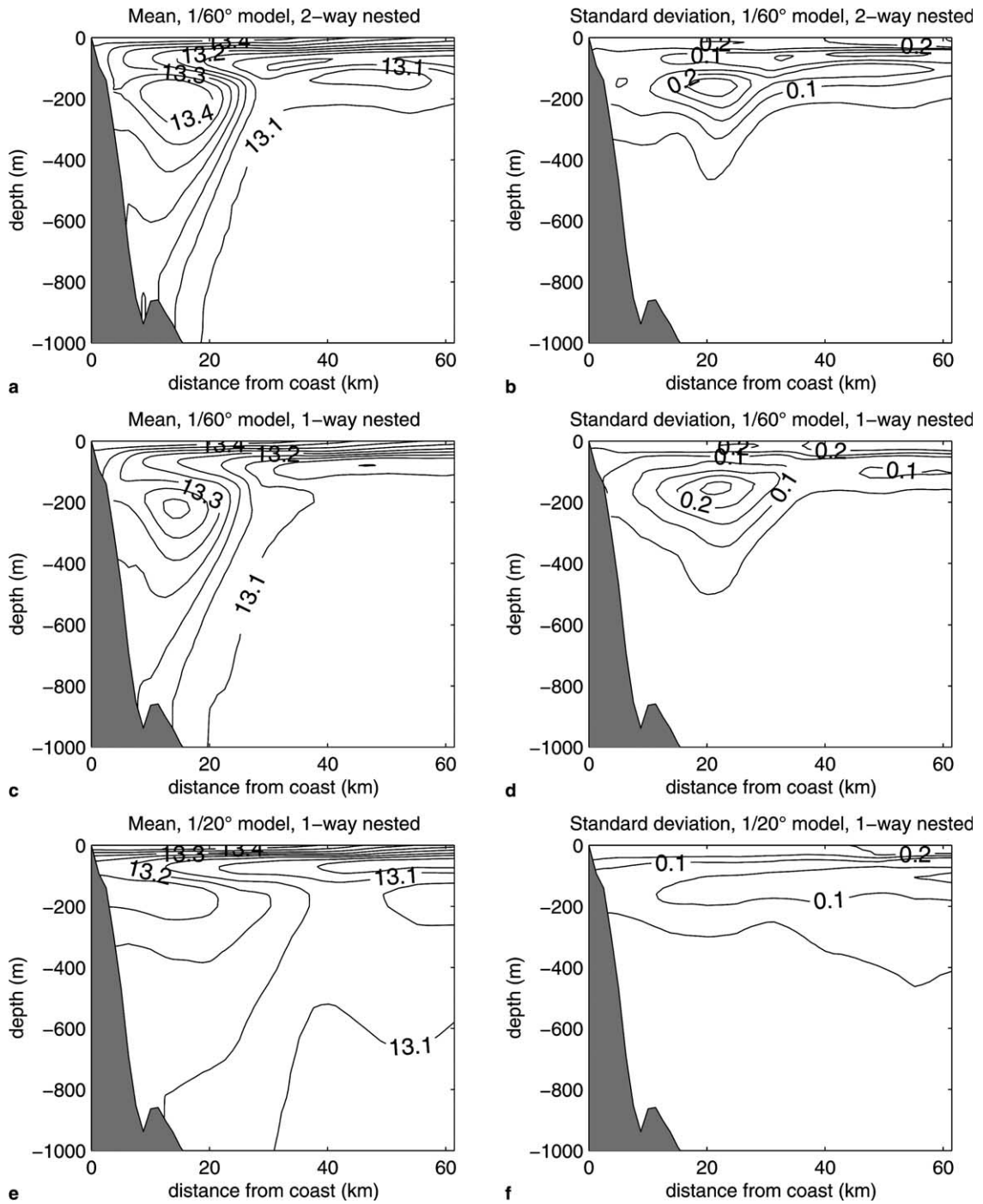
Fig. 4. Mean temperature and standard deviation (°C) at section C of Fig. 1 for the two-way (a and b) and the one-way nested model at 1/60° resolution (c and d). Panels (e) and (f) are the results of the 1/20° model for the one-way nesting strategy.

Fig. 4 shows temperature sections of the NC. The mean and the standard deviation of the temperature during the three winter months for the Ligurian Sea model in the two-way and one-way configuration and the Liguro-Provençal basin model in the one-way case are depicted. The extension and the temperature of the LIW vein is in all three cases smaller and colder than measured by Albérola et al. (1995). The clearest signal of the LIW is found for the two-way nested high-resolution model and the simulated properties of this vein are close to the observed values. In the one-way high-resolution model of the Ligurian Sea, the LIW core is still present, but the mean temperature is too low and the variability of this current is also lower than in the two-way nested model. With a three times coarser grid, the model was unable to simulate the LIW vein in the Ligurian Sea as can be seen on Fig. 4(e), and the LIW flows through the Liguro-Provençal model in a rather unstructured and unsteady manner. The fine grid was thus necessary to maintain the temperature gradient high between the LIW and the offshore water masses and to confine the NC to the coast. In the Gulf of Lions (covered by the 1/20° grid model) the structure of the NC is also better represented in the two-way nested system than in the one-way nested models. The feedback from the finer resolution model thus also improves the simulation at larger scale, not only in the region of feedback but also in remote places.

5. Results

We present here the results of a three-month integration, starting January 1st, 1998. The simulated transports and water properties of the three major currents (ECC, WCC and NC) are averaged over the integration period and are compared to results of surveys carried out in this region. The salinity and temperature gradient of the Liguro-Provençal front and the scale of mesoscale structures in the Ligurian Sea and the Gulf of Lions are also validated in the subsequent sections. The overall characteristics of the Ligurian
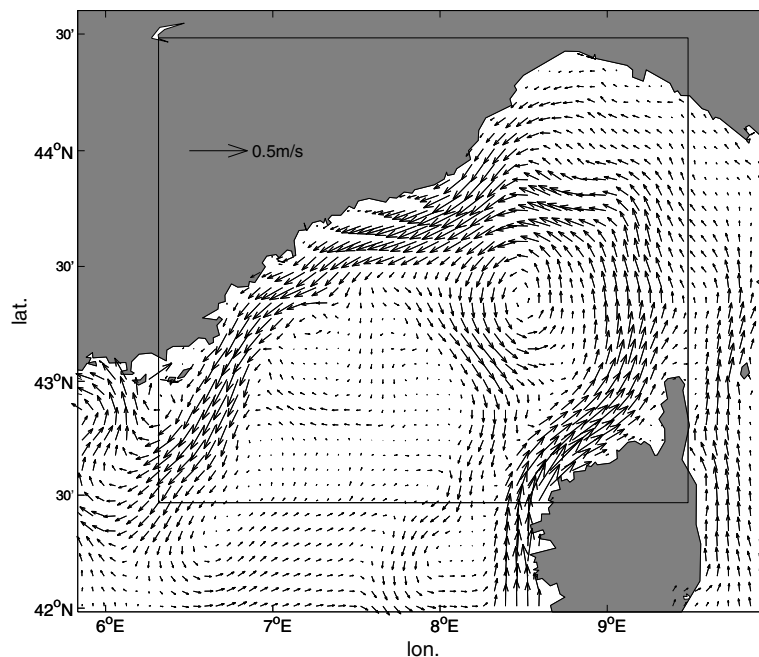

Fig. 5. Mean velocity in winter at the surface in the Ligurian Sea. The solid line represents the interface between the fine and intermediate grid resolution models.

Sea are well reproduced in the model. The signals of the ECC, WCC and the NC can clearly be seen in the surface velocity (Fig. 5). The transitions from 1′ to the 3′ model and from the 3′ to the 15′ model (not shown) are smooth for all variables.

5.1. The Eastern Corsican Current

The ECC flows to the north through the Corsican Strait up to a depth of 450 m and with a width of 35 km. Its intensity increases in spring and weakens in fall (Astraldi et al., 1999). The mean vertical structure of the simulated ECC at the strait of Corsica is shown in Fig. 6. The depth and the width are very close to the estimated values. A section in the salinity field shows that the MAW and the LIW are well present in the model. The order of magnitude of the velocity in the strait (0.2 m/s) reproduced by the model is in good agreement with the direct measurements (0.1–0.3 m/s). The simulated flows of MAW (from the surface to 200 m) and of LIW through the strait are 0.59 Sv (1 Sv = 10^6 m^3/s) and 0.38 Sv, respectively. These transports are comparable to annual mean transport based on measurements: 0.56 Sv for the surface flow and 0.14 Sv for the intermediate flow (Astraldi & Gasparini, 1992; Astraldi et al., 1999).

5.2. The Western Corsican Current

The WCC follows the Western Corsican Coast in its northward flow. It extends 30 km offshore and its depth reaches 600 m. The WCC transports about 1.15 Sv MAW into the Ligurian Sea. The transport is at a
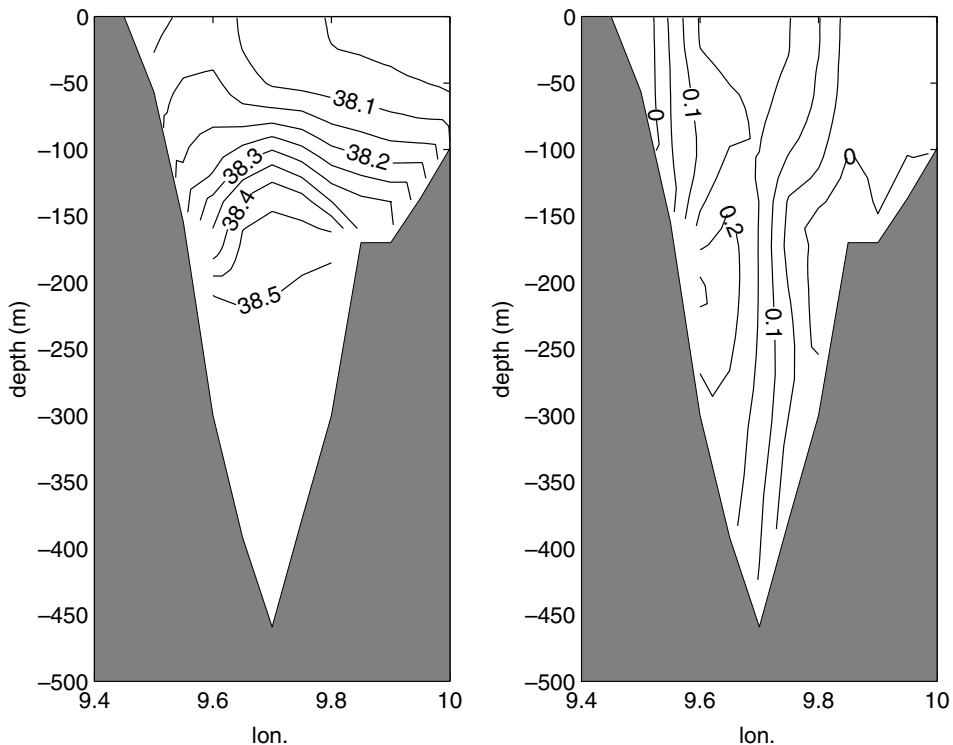

Fig. 6. Cross-section in the strait of Corsica (section A of Fig. 1) of the mean salinity and the mean zonal velocity (m/s) of the model. The two water masses MAW and LIW transported by the ECC can be seen in the salinity section.
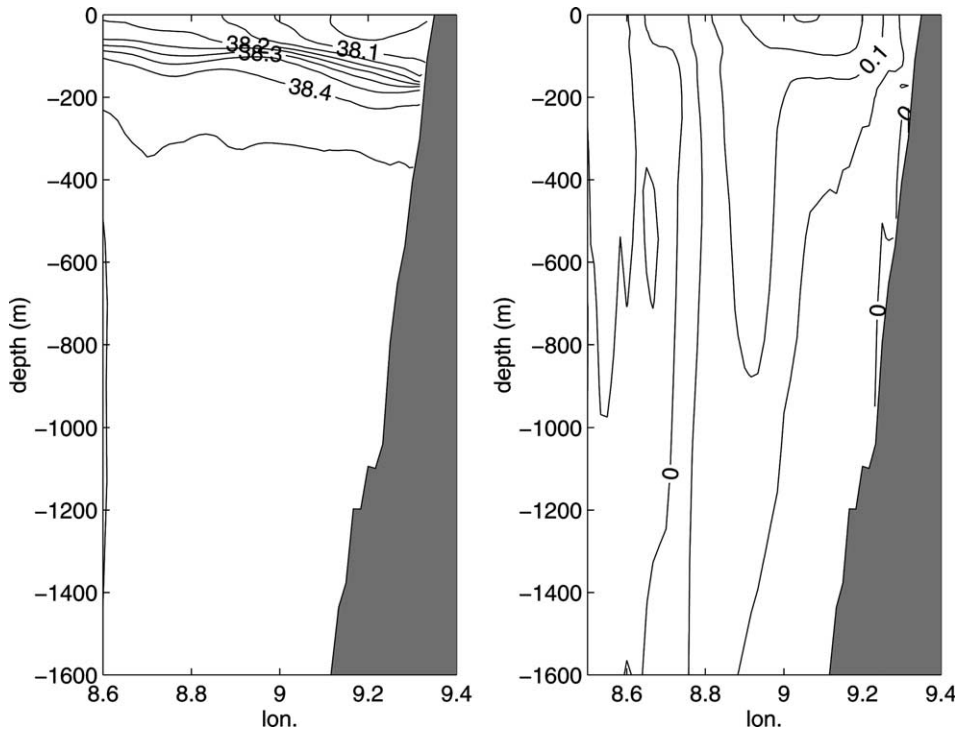
Fig. 7. Cross-section off the WCC (section B of Fig. 1) of the mean salinity and the mean zonal velocity (m/s) of the model.

maximum during spring. Typical velocities of the WCC range around 0.09 m/s (±0.06 m/s standard deviation) during winter (Astraldi & Gasparini, 1992; Sammari et al., 1995).

This current flows through all three models of the nesting system. Fig. 7 shows the N–S component of the WCC west of the Capo Rosso and the salinity at the same location. The depth (800 m) and the width (32 km) of the WCC are comparable to the depth obtained by measurements. An unphysical countercurrent next to the WCC can be found in the intermediate resolution model. This countercurrent is characterised by a maximum velocity of 0.2 m/s. Mean transport of the WCC during the model integration near the Capo Rosso was 1.22 Sv and is in good agreement with values of Astraldi and Gasparini (1992). However, a high variability of the WCC in position and strength was observed in the model. The steep bathymetry and the nesting boundaries transecting the topographic slope make the modelling of the WCC a delicate task.

5.3. The Northern Current

The NC is one of the major veins of the Western Mediterranean Sea. It takes birth in the Ligurian Sea and follows the continental slope until the Catalan Sea. Its width ranges from 20 km in winter to 30 km in summer. From late January to mid-March, the 0.1 m/s isotach is steep and deeper than 200 m. The transport of the upper 200 m ranges from 0.9 to 1.5 Sv. Below this level (between 200 and 700 m), only a weak transport of 0.2–0.4 Sv is measured. Generally, MAW can be found at the surface in the NC lying above a core of LIW located relatively close to the coast at 20–25 km and at depths of 400–500 m. Cooling and homogenisation of the MAW processes occur in winter and a relatively thin layer of WIW (T = 13.0–12.9 °C, S = 38.12–38.20) between 100 and 200 m is formed in late February (Albérola et al., 1995; Sammari et al., 1995).
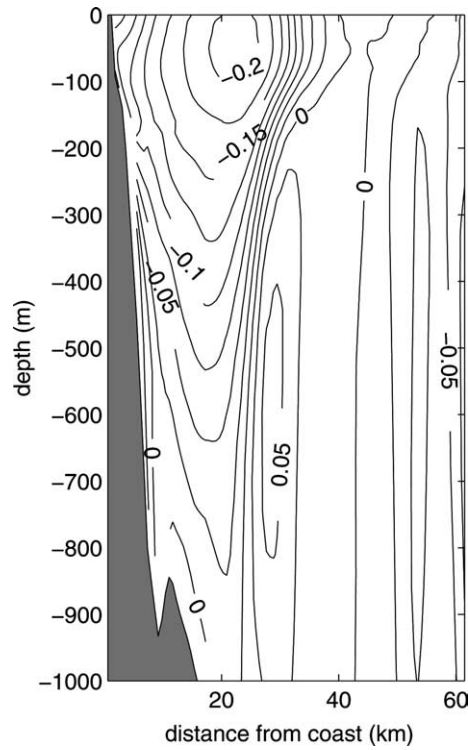
Fig. 8. Mean velocity (m/s and normal to the cross-section) of NC (section C of Fig. 1) in function of depth and distance from the coast.

In Figs. 4(a) and 8, cross-sections of the temperature and the normal velocity are shown. The velocity of NC (0.23 m/s) is lower than the estimation of the maximum velocity based on geostrophy (0.6 m/s, Sammari et al., 1995) and direct measurements (0.5 m/s, Albérola et al., 1995). The transports simulated by the model give satisfactory results at the surface (0.95 Sv for the first 200 m), while the transport of 0.12 Sv between 200 and 700 m is slightly lower than measurements by Sammari et al. (1995).

The signature of the different water masses is also well present in the model. The temperature section (Fig. 4(a)) very clearly displays the core of LIW advected by the ECC that joins the NC. At a depth of 100 m, a temperature minima characterising the presence of WIW is successfully reproduced by the model. Above the WIW, a layer of less modified and advected MAW can be observed in the model.

During wintertime the NC exhibits high mesoscale activity. This variability is associated with meanders of the NC due to baroclinic instabilities. The meanders have a typical wavelength of 30–60 km and propagate with a phase velocity of 10 km/day downstream. The fluctuations perpendicular to the coast are of a few tens of km and can thus affect the whole width of the current (Albérola et al., 1995; Sammari et al., 1995). The offshore displacement of the NC can be easily seen on Fig. 4(b) showing the standard deviation of the temperature. Since the temperature of LIW is very different from the surrounding water masses, the highest variability is located next to the core of LIW.

Fig. 9 shows a horizontal section of temperature at 200 m. Around the longitude 7°30′ and latitude 43°20′, we see the development of a meandering instability. Its wavelength is about 55 km. The phase velocity is more difficult to determine because different perturbations of the front with different phase velocity are overlaid. The phase velocities reproduced in the model are about 20 km/day.
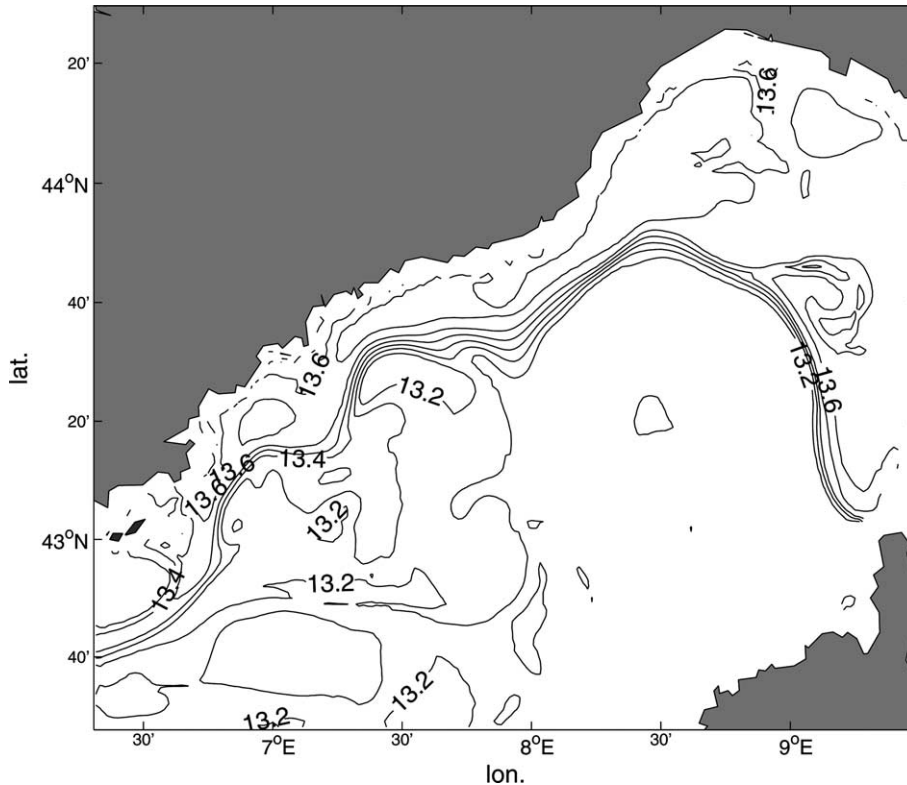
Fig. 9. Temperature (°C) at 200 m for April 20th, 1998 and meandering structures of the LIW vein.

The unstable path of the NC also favours the exchange between the LIW and the much colder and saltier offshore water masses. Filaments and eddies of LIW leave the main flow path of the NC and maintain their characteristic thermohaline properties for sometimes up to 20 days before they diffuse or return back to the main flow of the NC. The standard deviation of the temperature at a section of 200 m depth shows that the outbreak of LIW filaments and eddies often occurs in a region around 7°30′ longitude and 43°20′ latitude (Fig. 10). This might be due to the topographic feature at this location, which perturbs the NC following the continental slope. The topographic feature is characterised by the 2000 m isobath on Fig. 1. This plateau located in the continental slope extends about 15 km offshore.

Fig. 11 shows the transport of LIW crossing the section in the NC during the model integration. The high variability is due to interaction of the LIW vein with the offshore water masses. The sharp minimum at day 24 is due to a breaking of the LIW vein by offshore water. After this blockade is released, the LIW transport reaches its highest value observed during the model integration around day 50.

In the section where the transport of LIW was computed, another interesting process occurs. Surface cooling has produced a water mass called WIW, with a temperature of 12.9–13 °C and a salinity of 38.3–38.4 (Fig. 12). These rotating lenses of WIW (also called weddies) have been found in the Catalan Sea and in the Ligurian Sea (Gasparini et al., 1999). The characteristics of the simulated WIW lens agree with the observed range of temperature 12.5–13 °C and salinity 38.1–38.3 (Salat & Font, 1987). Particular to the present situation is its strong interaction with the vein of LIW broken into two branches. This caused a decrease of the LIW transport, as can be seen on Fig. 11 at day 64. During the three winter months the formation of eight WIW lenses has been observed, most of them in January.
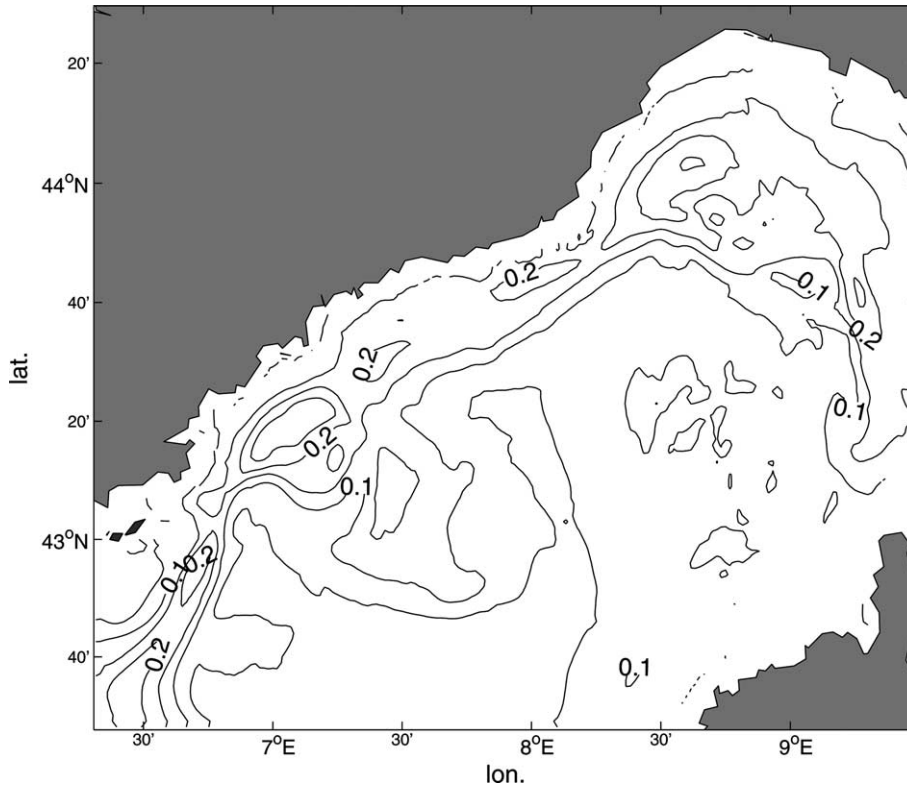
Fig. 10. Standard deviation of temperature (°C) at 200 m. The high variability of the NC near Nice might be due to topographic interactions.

5.4. The Liguro-Provençal front

The Liguro-Provençal front is formed by a high gradient in temperature and salinity separating coastal waters from those located offshore. Coastal waters are warmer (more than 14 °C) and less saline (about 38) than the interior waters, with temperatures below 13.8 °C and salinities of 38.1–38.2 (data collected in early spring at the Gulf of Genoa (Gasparini et al., 1999)). Other studies (e.g., Albérola et al., 1995) indicate that the vertical mixing occurring in winter leads to the homogenisation of the surface layer temperature in both the coastal and the interior waters. The winter surface temperature is about 13 °C, and these data are collected in a section of 55 km from the coast to the interior, starting near Nice.

The model simulates well the Liguro-Provençal front. Gradients are consistent, with a difference of about 0.3 °C and 0.2 between coastal and interior waters. Coastal waters show temperature and salinity values of about 13.3 °C and 38, and in the interior the values are of about 13 °C and 38.2, respectively, during winter. In early spring (March), the salinity rises by about 0.1 over the whole Ligurian Sea, but for temperature, similar values to those of Gasparini et al. (1999) are obtained. The temperature of the coastal zones ranges between 13.9 and 14.5 °C and between 13.6 and 13.7 °C in the interior of the basin (not shown). The Liguro-Provençal front can also be seen in remote sensed sea surface temperature (SST). Fig. 13 shows a composite advanced very high-resolution radiometers (AVHRR) SST for the March 23rd, 1998 and the corresponding model result. The model gives a quite satisfactory result, except near the Italian coast where the temperature is about 0.5 °C too low. Also the temperature at the surface is very smooth. This is due to the coarse resolution of the atmospheric heat flux.
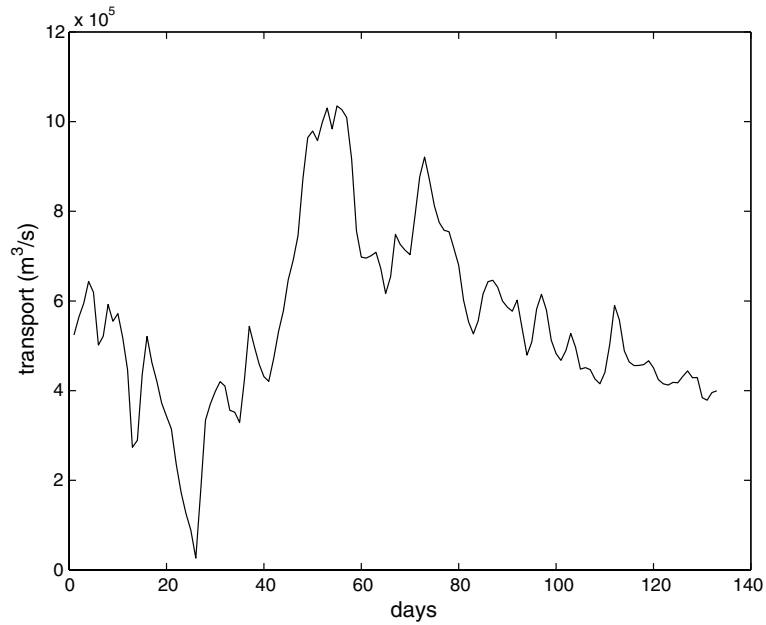
Fig. 11. The transport of LIW (m³/s) trough section D of Fig. 1 as a function of time (days). Water masses warmer than 13.4 °C and below 100 m were identified as LIW.
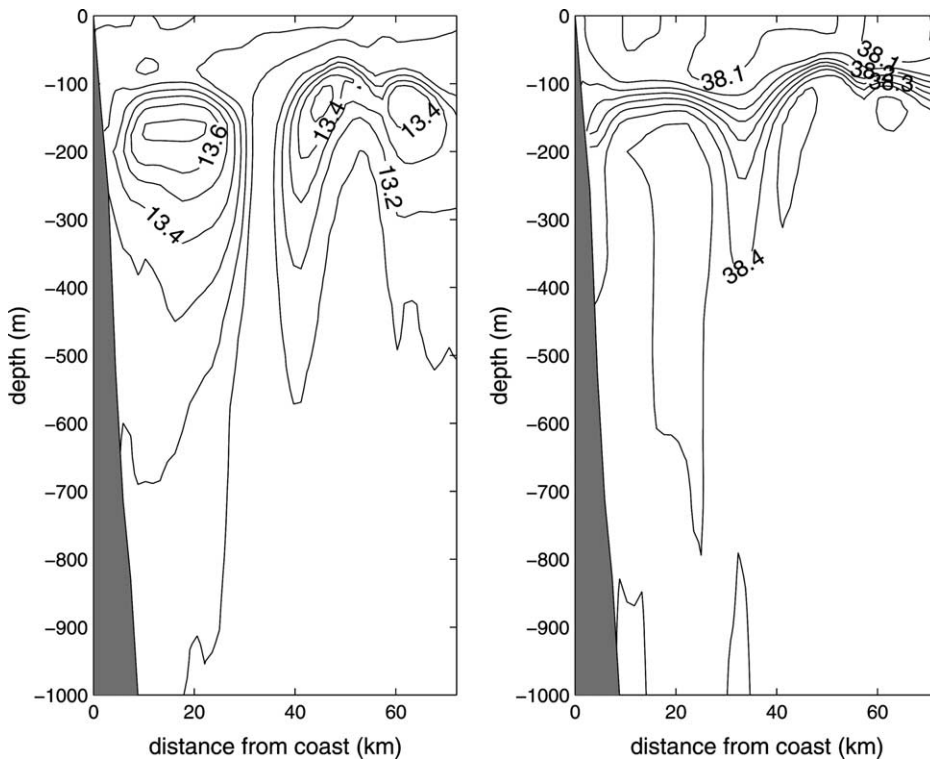

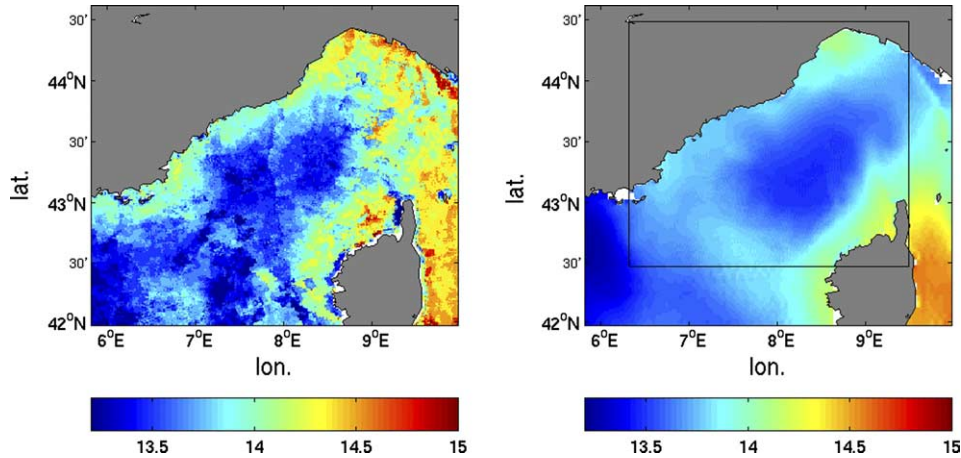Fig. 12. Temperature (°C) and salinity at section D of Fig. 1.

Fig. 13. Remotely sensed SST (AVHRR) and model SST (°C) for March 23rd, 1998.

6. Conclusions

A complex nesting system was implemented at three different resolutions in the Mediterranean Sea. Two successive zooms are performed to study small-scale processes of the Ligurian Sea. At a reasonable cost it was thus possible to set up a model of 1′ resolution of the Ligurian Sea by avoiding the open boundary problem. The two-way nesting approach appears to be an effective and robust method for simulating oceanographic systems at variable resolutions. The Northern Current is better represented in the two-way nested model than in a coarser resolution grid and in the one-way nested model. The improvement was not only observed in the region covered by the high-resolution model, but also downstream in the coarse resolution model. The interaction between small-scale processes and larger scale currents and fronts are taken into account: meanders and eddies induced by instabilities of basin-wide currents and fronts are well observed in the intermediate and fine grid models. No particular problems were observed at the nesting boundaries. Due to the feedback and the sponge layer, the transition between the finer and the coarser grid model is smooth and confirms the robustness of the adopted nesting procedure.

The nesting system was able to simulate the major characteristics of the Ligurian Sea and the Liguro-Provençal basin. The three coastal currents influencing this area are present in the model at position, width and depth comparable to those obtained from different surveys. The transports of the Western Corsican Current (WCC), the Eastern Corsican Current (ECC) and the Northern Current (NC) are also consistent with values computed from observations. Especially, the transports of the WCC and the ECC are in very good agreement with previous measurements (Astraldi & Gasparini, 1992; Astraldi et al., 1999; Sammari et al., 1995). However, a countercurrent next to the WCC is formed. This countercurrent is, to our knowledge, not observed and could be an artefact of the interpolation of the boundary condition. This current seems to weaken the NC and should be further analysed.

Appendix 1. Nesting procedure

1.1. Boundary conditions

The integration of the fine grid model requires boundary conditions for horizontal velocity, temperature, salinity and turbulent kinetic energy. The interpolation of these boundary conditions is performed for each vertical level independently.

1.1.1. Normal velocity

The velocity component normal to the boundary has the greatest impact on the flow inside the fine grid model. Fine grids and coarse grids are staggered in a way that the interpolation of the normal velocity requires only an interpolation tangent to the boundary. The boundary conditions of the normal velocity are extracted and imposed in column C of Fig. 2.

We note $\mathbf{x}_{\mathbf{v}_n}^{\mathrm{c}}$ the vector formed by the N normal velocity components of the coarse grid model of a given boundary segment and of a given layer and $\mathbf{x}_{\mathbf{v}_n}^{\mathrm{f}}$ the corresponding unknown velocity components of the fine grid. The volume conservation constraint can be formulated by a linear relationship

$$\mathbf{x}_{\mathbf{v}_n}^{\mathrm{c}} = \mathbf{R}\mathbf{x}_{\mathbf{v}_n}^{\mathrm{f}}, \tag{1}$$

where $\mathbf{R}$ is a $N \times rN$ matrix given by

$$\mathbf{R}_{i,j} = \frac{\Delta z_j^{\mathrm{f}}}{r\Delta z_i^{\mathrm{c}}} \quad \text{if } r_i \in \{j, j, +1 \cdots j + r - 1\} \text{ and if the } i\text{th coarse grid box is a sea box} \tag{2}$$

$$= 0 \quad \text{elsewhere} \tag{3}$$

where Δz_j^{f} and Δz_i^{c} are the vertical grid spacing of the fine and coarse mesh, respectively. The boundary conditions of the normal velocity for the fine grid should be smooth, but in any case the volume conservation must be satisfied. $\mathbf{x}_{\mathbf{v}_n}^{\mathrm{f}}$ is obtained by minimising the cost function $J(\mathbf{x}_{\mathbf{v}_n}^{\mathrm{f}})$, penalising abrupt variations under the constrain of conservation (Eq. (1))

$$J(\mathbf{x}_{\mathbf{v}_n}^{\mathrm{f}}) = (\mathbf{L}\mathbf{x}_{\mathbf{v}}^{\mathrm{f}})^{\mathrm{T}}(\mathbf{L}\mathbf{x}_{\mathbf{v}_n}^{\mathrm{f}}), \tag{4}$$

where $\mathbf{L} \in \mathfrak{R}^{(N-2) \times N}$ is the discrete second derivative operator. The solution of this minimisation problem is given in Appendix 2. This interpolation method can be generalised in order to relax the constraint that the land mask of the fine grid and coarse grid must be equal at the boundary. By a suitable definition of the reduction operator $\mathbf{R}$, any fine grid land mask can be treated.

1.1.2. Tangent velocity

The velocity tangent to the boundary only plays a part in the horizontal mixing and advection of momentum. These terms are generally small compared to the other forces. The tangent velocity component at the fine grid boundary (column B) is therefore obtained by a simple bilinear interpolation using the four

nearest tangent velocity components of the coarse grid (columns A and D). No volume conservation aspects must be taken into account for this velocity component.

1.1.3. Scalars

In a first step, temperature, salinity and turbulent kinetic energy are linearly interpolated normally to the boundary (from columns A and D to column B). Then, these values are interpolated tangentially to the boundary using a similar interpolation formula as the normal velocity. For the scalars we impose a constraint independent of the sigma-layer thickness

$$\mathbf{R}_{i,j} = \frac{1}{r} \quad \text{if } r_i \in \{j, j+1 \cdots + j + r - 1\} \quad \text{and if the } i\text{th coarse grid box is a sea box,} \tag{5}$$

$$= 0 \quad \text{elsewhere.} \tag{6}$$

This procedure is obviously not conservative. The design of a stable and flux conservative interpolation is not trivial, since a smooth flux boundary condition does not guarantee a resulting smooth scalar field.

1.2. Feedback

After each time step the mean values of the fine grid mesh replace the values of the coarse grid model of the overlapping region. The velocity components are averaged over the interfaces of the corresponding coarse grid box. For the scalar variables (elevation, temperature, salinity and turbulent kinetic energy), the mean values over the whole coarse grid box are taken.

For stability reasons, some authors (e.g., Fox & Maskell, 1995; Ginis et al., 1998) separate the feedback interface from the dynamic interface. Here, no such problems occur and the feedback interface was chosen as close as allowed by the grid configuration to the dynamic interface.

In the present case, it would be sufficient to apply the feedback only to the first coarse grid boxes inside the overlapping region, since the feedback is performed every time step for both barotropic and baroclinic modes, and for a one-time step forecast every grid box depends, at the first order, only on its direct neighbourhood.

1.3. Sponge layer

It is natural to attribute to the coarse resolution model a higher diffusion than the diffusion of the fine grid model. At the boundary and over a distance of two coarse grid boxes, the diffusion in the fine grid model is raised linearly to reach the diffusion of the coarse resolution model. The utility of a sponge layer for embedded models is justified by the following reasons:

- Small scale features (compared to the grid spacing of the coarse model) moving outward the fine grid model cannot properly be resolved by the coarse grid model. These features are thus damped by the sponge layer.
- The behaviour of the coarse grid model is necessarily different than that of the fine grid model. For example, the advection speed of a perturbation depends on the grid spacing (Miyakoda, 2002). Thus, boundary conditions for the fine grid model are never perfect and totally consistent with the fine model dynamics. The sponge layer regularises the reaction of the fine grid model to imperfect boundary conditions.
- The hydrostatic inviscid primitive equations with open boundaries are mathematically ill posed (Browning, Holland, Kreiss, & Worley, 1990; Oliger & Sundstrom, 1978). For one-way nesting, diffusion (or some other special treatment) is thus necessary at the boundaries. But a priori it is not clear if this problem occurs to the same extent in a two-way nested model.

More sophisticated solutions have been proposed to regularise the behaviour of the fine grid model at the boundary, e.g., the radiative-nesting Boundary Conditions of Chen (1991), a flow relaxation scheme (Oey & Chen, 1992), a Newtonian-type damping scheme (Kurihara & Bender, 1980). But most of these methods alter the volume transport inside the fine grid, and are therefore not considered here.

Appendix 2. Interpolation procedure for the normal velocity

The dynamics inside the fine grid domain strongly depend on the velocity component normal to the boundary. An accurate interpolation scheme is thus desirable. Smooth boundary conditions for the fine grid $\mathbf{x}^{\mathrm{f}}_{\mathbf{v}_n}$ can be obtained by minimising the following cost function:

$$J(\mathbf{x}^{\mathrm{f}}_{\mathbf{v}_n}) = (\mathbf{L}\mathbf{x}^{\mathrm{f}}_{\mathbf{v}_n})^{\mathrm{T}}(\mathbf{L}\mathbf{x}^{\mathrm{f}}_{\mathbf{v}_n}), \tag{7}$$

under the constraint

$$\mathbf{x}^{\mathrm{c}}_{\mathbf{v}_n} = \mathbf{R}\mathbf{x}^{\mathrm{f}}_{\mathbf{v}_n}, \tag{8}$$

where $\mathbf{L} \in \mathfrak{R}^{(N-2)\times N}$ is the discrete second derivative ($\delta_{ij} = 1$ if $i = j$ and 0 otherwise)

$$\mathbf{L}_{i,j} = \delta_{i,j-1} - 2\delta_{i,j} + \delta_{i,j+1}. \tag{9}$$

An application of a minimisation using Lagrangian multipliers would require the inverse of the singular matrix, $\mathbf{L}^{\mathrm{T}}\mathbf{L}$. The singularity is due to the fact that the cost function does not depend on a constant shift and a constant slope of $\mathbf{x}^{\mathrm{f}}_{\mathbf{v}_n}$. It is therefore preferable to identify the vector space constrained by the volume conservation and the unconstrained null space of $\mathbf{R}$. The basis vectors of the former space are columns of the matrix $\mathbf{V} \in \mathfrak{R}^{rN \times N}$ and the basis vector of the latter are the columns of $\mathbf{V}^0 \in \mathfrak{R}^{rN \times (r-1)N}$. One can then decompose $\mathbf{x}^{\mathrm{c}}_{\mathbf{v}_n}$ into

$$\mathbf{x}^{\mathrm{f}}_{\mathbf{v}_n} = \mathbf{V}_{\mathbf{c}}\mathbf{a}_{\mathbf{c}} + \mathbf{V}_0\mathbf{a}_0. \tag{10}$$

The components in the constrained space are directly given by (8)

$$\mathbf{a}_{\mathbf{c}} = (\mathbf{R}\mathbf{V}_{\mathbf{c}})^{-1}\mathbf{x}^{\mathrm{c}}_{\mathbf{v}_n}. \tag{11}$$

By minimising the square of the second derivative of the boundary condition, one obtains then the remaining components

$$\mathbf{a}_0 = -(\mathbf{V}_0^{\mathrm{T}}\mathbf{L}^{\mathrm{T}}\mathbf{L}\mathbf{V}_0)^{-1}\mathbf{V}_0^{\mathrm{T}}\mathbf{L}^{\mathrm{T}}\mathbf{L}\mathbf{V}_{\mathbf{c}}(\mathbf{R}\mathbf{V}_{\mathbf{c}})^{-1}. \tag{12}$$

Finally, the boundary conditions applied to the fine grid mesh yield

$$\mathbf{x}^{\mathrm{f}}_{\mathbf{v}_n} = (\mathbf{I} - \mathbf{V}_0(\mathbf{V}_0^{\mathrm{T}}\mathbf{L}\mathbf{V}_0)^{-1}\mathbf{V}_0^{\mathrm{T}}\mathbf{L}^{\mathrm{T}}\mathbf{L})\mathbf{V}_{\mathbf{c}}(\mathbf{R}\mathbf{V}_{\mathbf{c}})^{-1}\mathbf{x}^{\mathrm{c}}_{\mathbf{v}_n}. \tag{13}$$

For an efficient implementation of the interpolation procedure, the interpolation coefficients are computed once and stored.

References

Albérola, C., Millot, C., & Font, J. (1995). On the seasonal and mesoscale variabilities of the Northern Current during the PRIMO-0 experiment in the Western Mediterranean Sea. *Oceanologica Acta, 18*, 163–192.

Astraldi, M., & Gasparini, G. P. (1992). The seasonal characteristics of the circulation in the north Mediterranean basin and their relationship with the atmospheric-climatic conditions. *Journal of Geophysical Research, 97*, 9531–9540.

Astraldi, M., Balopoulos, S., Candela, J., Font, J., Gacic, M., Gasparini, G. P., Manca, B., Theocharis, A., & Tintoré, J. (1999). The role of straits and channels in understanding the characteristics of Mediterranean circulation. *Progress in Oceanography, 44*, 65–108.

Beckers, J.-M. (1991). Application of a 3D model to the Western Mediterranean. *Journal of Marine Systems, 1*, 315–332.

Beckers, J.-M., Rixen, M., Brasseur, P., Brankart, J.-M., Elmoussaoui, A., Crépon, M., Herbaut, Ch., Martel, F., Van den Berghe, F., Mortier, L., Lascaratos, A., Drakopoulos, P., Korres, P., Pinardi, N., Masetti, E., Castellari, S., Carini, P., Tintore, J., Alvarez, A., Monserrat, S., Parrilla, D., Vautard, R., & Speich, S. (2002). Model intercomparison in the Mediterranean. The MEDMEX simulations of the seasonal cycle. *Journal of Marine Systems, 33–34*, 215–251.

Blayo, E., & Debreu, L. (1999). Adaptive mesh refinement for finite difference ocean model: some first experiments. *Journal of Physical Oceanography, 29*(6), 1239–1250.

Brasseur, P., Beckers, J.-M., Brankart, J.-M., & Schoenauen, R. (1996). Seasonal temperature and salinity fields in the Mediterranean Sea: climatological analyses of an historical data set. *Deep Sea Research, 43*(2), 159–192.

Browning, G. L., Holland, W. R., Kreiss, H.-O., & Worley, S. J. (1990). An accurate hyperbolic system for approximately hydrostatic and incompressible oceanographic flows. *Dynamics of Atmospheres and Oceans, 14*, 303–332.

Chen, C. (1991). A nested grid, nonhydrostatic, elastic model using a terrain following coordinate transformation: the radiative-nesting boundary conditions. *Monthly Weather Review, 119*, 2851–2869.

Fox, A. D., & Maskell, S. J. (1995). Two-way interactive nesting of primitive equation ocean models with topography. *Journal of Physical Oceanography, 25*, 2977–2996.

Fox, A. D., & Maskell, S. J. (1996). A nested primitive equation model of the Iceland Faeroe front. *Journal of Geophysical Research, 101*, 18259–18278.

Gasparini, G. P., Zodiatis, G., Astraldi, M., Galli, C., & Sparnocchia, S. (1999). Winter intermediate water lenses in the Ligurian Sea. *Journal of Marine Systems, 20*, 319–332.

Ginis, I., Richardson, R. A., & Rothstein, L. M. (1998). Design of a multiply nested primitive equation ocean model. *Monthly Weather Review, 126*, 1054–1079.

Kurihara, Y., & Bender, M. A. (1980). Use of a movable nested-mesh model for tracking a small vortex. *Monthly Weather Review, 108*, 1792–1809.

Miyakoda, K. (2002). Strategy for regional seasonal forecasts. In N. Pinardi & J. Woods (Eds.), *Ocean forecasting: Conceptual basis and applications* (pp. 179–198). Berlin: Springer.

Nihoul, J. C. J., Deleersnijder, E., & Djenidi, S. (1989). Modelling the general circulation of Shelf Seas by 3D k–ε models. *Earth-Science Reviews, 26*, 163–189.

Oey, L.-Y., & Chen, P. (1992). A nested-grid ocean model: with application to the simulation of meanders and eddies in the norwegian coastal current. *Journal of Geophysical Research, 97*(C12), 20063–20086.

Oliger, J., & Sundstrom, A. (1978). Theoretical and practical aspects of some initial and boundary value problems in fluid dynamics. *SIAM Journal of Applied Mechanics, 35*(3), 419–446.

Rixen, M., Beckers, J. M., Brankart, J.-M., & Brasseur, P. (2000). A numerically efficient data analysis method with error map generation. *Ocean Modelling, 2*(1–2), 45–60.

Robinson, A. R., & Sellschopp, J. (2002). Rapid assessment of the coastal ocean environment. In N. Pinardi & J. Woods (Eds.), *Ocean forecasting: Conceptual basis and applications* (pp. 199–230). Berlin: Springer.

Rowley, C., & Ginis, I. (1999). Implementation of a mesh movement scheme in a multiply nested ocean model and its application to air-sea interaction studies. *Monthly Weather Review, 127*, 1879–1896.

Salat, J., & Font, J. (1987). Water mass structure near and offshore the Catalan coast during the winters of 1982 and 1983. *Annales Geophysicae, 1*, 49–54.

Sammari, C., Millot, C., & Prieur, L. (1995). Aspects of the seasonal and mesoscale variabilities of the Northern Current in the Western Mediterranean Sea inferred from the prolig-2 and pros-6 experiments. *Deep-Sea Research I, 42*(6), 893–917.

Smith, W. H. F., & Sandwell, D. T. (1997). Global sea floor topography from satellite altimetry and ship depth soundings. *Science, 277*, 1956–1962.

Spall, M. A., & Holland, W. R. (1991). A nested primitive equation model of oceanic application. *Journal of Physical Oceanography, 21*, 205–220.

Spall, M. A., & Robinson, A. R. (1989). A new open-ocean hybrid coordinate primitive equation model. *Mathematics and Computers in Simulation, 31*, 241–269.

Tusseau, M. H., & Mouchel, J. M. (1994). Nitrogen inputs to the Gulf of Lions via the Rhône river. In J. M. Martin & H. Barth (Eds.), *Water pollution research reports, proceedings of the EROS 2000 workshop, Hamburg, March 1994*. Commission of the European Communities

Zavatarelli, M., & Pinardi, N. (2003). The Adriatic Sea Modelling System : A nested approach. *Annales Geophysicae, 21*, 345–364.